ELSEVIER

Journal of Organometallic Chemistry 648 (2002) 155–163

Journal of Organometallic Chemistry

www.elsevier.com/locate/jorganchem

A theoretical study of the reaction products created by irradiation of the carbonyl iron silyl complexes $Cp(CO)_2FeSiH_2Me$ and $Cp(CO)_2FeCH_2SiH_3$

Damien Moigno [a], Ioana Pavel [a], Wolfgang Kiefer [a,*], Heinrich Jehle [b], Wolfgang Malisch [b]

[a] *Institut für Physikalische Chemie, Universität Würzburg, am Hubland, D-97074 Würzburg, Germany*
[b] *Institut für Anorganische Chemie, Universität Würzburg, am Hubland, D-97074 Würzburg, Germany*

Received 25 July 2001; received in revised form 10 September 2001; accepted 8 October 2001

Dedicated to Professor Manfred Christl on the occasion of his 60th birthday

Abstract

The theoretical reaction pathways of the irradiation of $Cp(CO)_2FeSiH_2CH_3$ and $Cp(CO)_2FeCH_2SiH_3$ have been studied by means of DFT calculations using the BPW91/6-311G* method. Although the calculated characteristic vibrational modes of the metal ligand unit for the various photoproducts are significantly different in constitution, they are very similar in wavenumbers, which did not simplify their identification. In spite of this, the theoretical results are found to be consistent with recent experimental findings obtained by the matrix isolation technique. © 2002 Published by Elsevier Science B.V.

Keywords: DFT-calculations, Matrix isolation; FT-IR and Raman spectroscopy; Photochemistry; Silyl metal complexes, agostic interaction

1. Introduction

Silyl iron complexes of the type $Cp(CO)_2Fe–SiH_2R$ (Cp = Cyclopentadienyl); (R = H (**1**), Me (**2a**)) offer a large synthetic potential in inorganic and organometallic chemistry [1]. Base-free transition-metal silylene complexes represent unusual organometallic species insofar as they possess a Lewis acidic center directly bound to the transition metal [2–4]. Several examples of base free silylene complexes of iron [3], ruthenium [5], tungsten [6] and osmium [7] have been synthesized. For complexes with $Fe{=}SiR_2$ U, heteroatom substitution on the silicon guarentees the isolation of these complexes. With the matrix isolation technique it should be possible to identify silylene complexes with the silicon bearing organic groups, hydrogen or halogen, respectively [8,9]. In previous works [10–12], some of us reported on FT–IR and Raman studies by means of the matrix isolation technique in order to obtain information on the photodecomposition of **1** and **2a**. The Raman spectrum of **1**, whose assignment was supported by DFT calculations, clearly shows that UV irradiation leads to a CO loss followed by an intramolecular rearrangement to generate primarily a 16-electrons and secondarily a stabilized 18-electrons species [10]. Besides the α-H-transfer in analogy to **1** (pathway A) in the methyl substituted silyl complex **2a**,

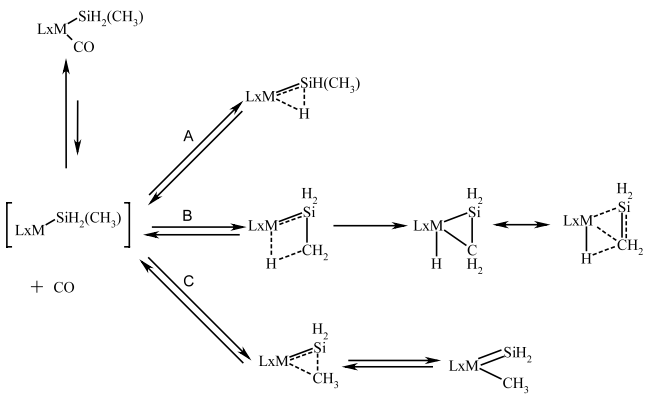

Scheme 1.

* Corresponding author. Tel.: +49-931-888-6330; fax: +49-931-888-6332.
E-mail address: wolfgang.kiefer@mail.uni-wuerzburg.de (W. Kiefer).

0022-328X/02/$ - see front matter © 2002 Published by Elsevier Science B.V.
PII: S0022-328X(01)01469-3

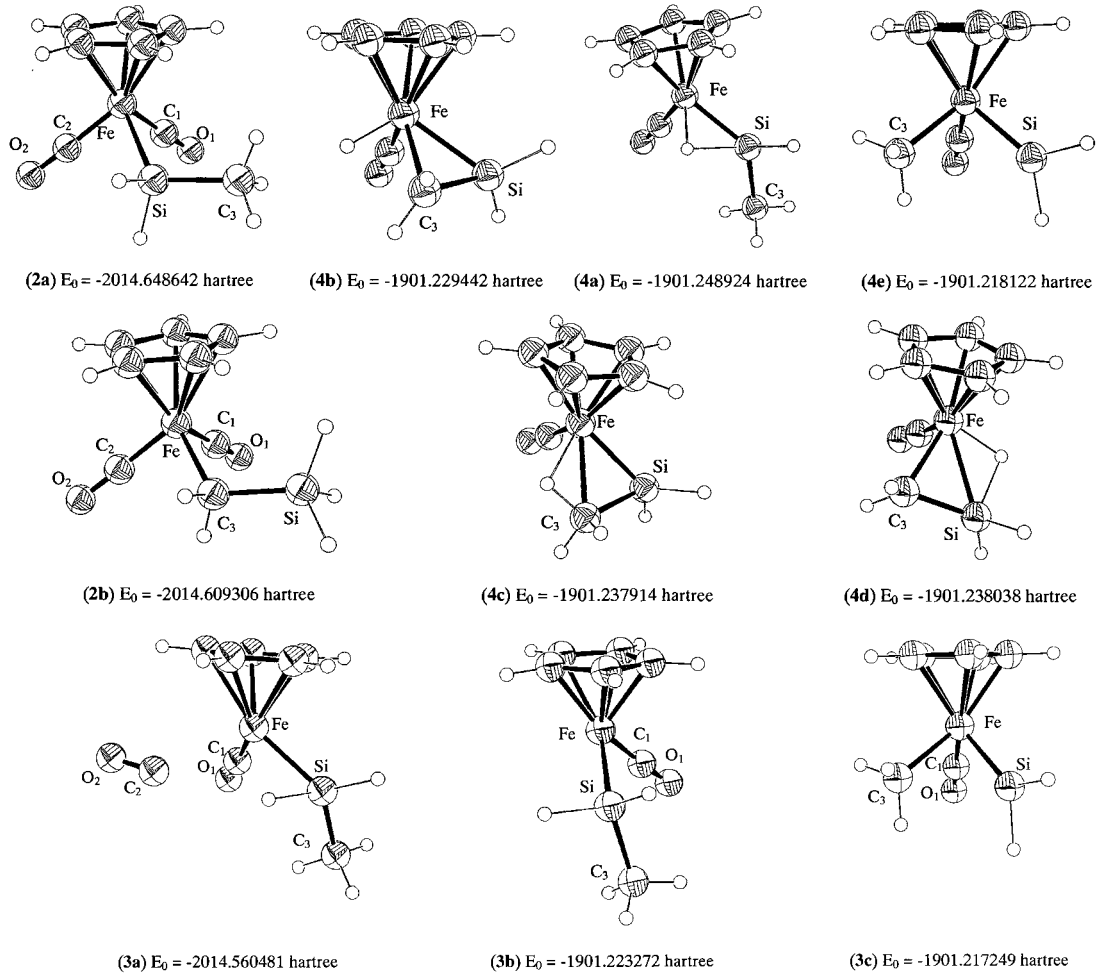

Fig. 1. Optimized geometries at BPW91/6-311G* of the iron complexes.

two further mechanisms for the photochemical conversion are plausible as depicted in Scheme 1. The reaction pathway B involves a β-H abstraction, whereas an oxidative addition of the Si–C bond to the metal is characteristic for pathway C. From the various possible photoproducts of **2a**, Fickert et al. [11,12] have proposed the α-H rearrangement as the most probable one (pathway A, Scheme 1) by comparing the Raman spectra of irradiated complexes **1** and **2a**. It has been shown that under normal condition, UV irradiation of **2a** leads after elimination of silylene (via pathway A, see Scheme 1) or silaethene (via pathway B, see Scheme 1), and CO addition, to the final photoproduct $[Cp(CO)_2FeH]$ (**5**), which is thermolabile and transforms to $[Cp(CO)_2Fe]_2$ [13]. Earlier, Gerhartz et al. [14] have shown that the photoexcitation of the complex $Cp(CO)_2Fe(C_2H_5)$ yields $Cp(CO)_2FeH$ (**5**) even at 10 K in an Ar matrix and that **5** shows two characteristic ν(CO) vibrational modes at 2024 and 1967 cm^{-1}. One may notice, that $Cp(CO)_2FeH$ (**5**) could à priori be generated via pathway A from 4a (Fig. 1) or via pathway B from **4b**–**c** (Fig. 1), where two bonds have to be simultaneously broken with a CO coordination.

The characterization of the isolated photoproduct(s) by spectroscopical methods is still a subject of discussion. Therefore, DFT calculations have been performed in order to explore the theoretical reaction pathways of $Cp(CO)_2Fe–SiH_2Me$ in the electronic ground state and to bring additional information to the experimental results. Since the irradiation of $Cp(CO)_2Fe–CH_2SiH_3$ (**2b**) should lead to **4d**, an isomeric form of **4c**, its molecular properties and photolysis products have also been determined theoretically. In addition, energy and vibrational modes with IR and Raman intensities were calculated. Particularly, transition states and intermediate species along the reaction pathways were determined and characterized to further elucidate the decay dynamics of **2a**–**b**.

2. Results and discussion

Fig. 1 displays the different rearranged 18 electron complexes **4a**–**e**, mentioned in Scheme 1. The expected 16 electron transition-states **3a**–**3c** (TS) were calculated with the STQN method of the GAUSSIAN program [15]. One imaginary vibrational mode for each of **3a**–**c** were determined at -411, -70 and -154 cm^{-1}, respectively.

The calculated energy of **4c** with the BPW91/6-311G* method is predicted to be 37.2 kJ mol^{-1} lower than **4e**, 22.2 kJ mol^{-1} lower than **4b** and 28.9 kJ mol^{-1} higher than **4a**. Using the same method, the **3a** and **3b** transition structures were found to be 45.6 and 69.4 kJ mol^{-1} energetically higher than **4a**. Additionally, the Cp(CO)(SiH_2Me)Fe–CO bond dissociation energy of **2a** was theoretically determined on the BPW91/6-311G* level. As expected, the $D_o = 186.2$ kJ mol^{-1} calculated value was very similar to that of the corresponding M–CO cleavages in $Fe(CO)_5$ [16].

Comparing the calculated structures of **4a** and **4c**, we notice interesting discrepancies in the metal–silicon bonding. While the Fe–Si bond length in **4a** is about 20 pm shorter in comparison with **2a**, the calculations indicate a shortage of 10 pm for **4c**. At the same time, the calculated Fe–H bond lengths in **4a** and **4c** are 161.0 and 176.1 pm, respectively. The much shorter iron–hydrogen interatomic distance in $Cp(CO)_2FeH$ (**5**) of 149.9 pm could represent a good bond order reference in this case. As shown in Fig. 1, the complexes **4a**, **4c** and **4d** are stabilized with agostic interactions [17]. The modification of the Z-Matrix for **4c** and reoptimization of the geometry have led to the compound **4b**, that represents a local minimum of the potential energy surface with a higher energy difference of 15.1 kJ mol^{-1} with respect to **4c**. For **4a**, no such compound was found and the optimization conducted systematically back to the more stable compound **4a**. Compound **4b** is the result of the H-β-shift addition on iron. The calculated Fe–H bond length of 148.5 pm corresponds well to the iron hydrid bond length calculated for **5**. Compared with **4c**, the Fe–Si and the Fe–C bonds are in this case about 9 pm longer and 14 pm shorter, respectively. Compound **4c** is stabilized by the β-H-agostic C–H–Fe-interaction, depicted in Fig. 1. In this context it should be mentioned that the Si=C bond distance has been determined in $H_2Si{=}CH_2$ [18] and $(CH_3)_2Si{=}CH_2$ [19] to be at 170.4 and 169.2 pm, respectively. Moreover, silaethene coordinated to ruthenium [20] and tungsten [21] is found to have a value for the Si–C bond length of 179.0 and 180.0 pm, respectively. The Si–C interatomic distance in **4b** was calculated in this study to be 180.7 pm, which is in good agreement with these cited experimental results. The Si–C bond length in **4c** is calculated to be 191.0 pm, which indicates a considerable Si–C single-bond character, so that **4c** can be described as a pseudo metallasilacyclopropane compound similarly to the model proposed by Dewar [22], Chatt and Duncanson [23] for the ethylene complexes.

Compound **4e** represents the photoproduct expected in the reaction pathway C. The Fe–Si bond length of 211.4 pm, which shows a d_π–p_π character, is only 1 pm shorter than in **4a**. The Fe–C_{Me} interatomic distance is calculated to be 206.8 pm. Further relevant parameters of compounds **2a**–**4e** and **5**, calculated with the BPW91 functional and the 6-311G* basis set, are listed in Table 1. The calculations have shown that compound **4a** is thermodynamically the most stable one, therefore, it should be the favored compound in the matrix layer. But, by the photolysis carried out using wavelengths in the range between 364 and 333 nm, an energy of 330.2–359.5 kJ mol^{-1} was deposited on the parent molecule. According to the theoretical results, there is sufficient energy to overcome the transition states **3a**–**c**. Consequently, the previously discussed reaction pathways could be valid.

Fickert et al. [11,12] showed that the photochemical conversion was not complete and an increase of the irradiation time will produce no further changes. Therefore, they suggested an equilibrium between the silyl complex **2a** and the transition state **3a** during photochemical conversion, a phenomenon that has already been observed. For example, the UV photolysis of $Fe(CO)_5$ in an argon matrix leads to $Fe(CO)_4$ and CO. Subsequent exposure of the matrix to the light from the Nernst glower of the IR spectrometer rapidly destroys all the $Fe(CO)_4$ and regenerates the parent $Fe(CO)_5$ [24]. If the UV photolysis is continued for several hours, it is found that the reaction can be only partially reversed. Prolonged photolysis allows the CO to diffuse away through the matrix layer until a definite concentration is reached, preventing subsequent recombination. The UV light used for the photolysis contains far more energy than is required to break the M–CO bond. Since no visible fluorescence is observed in these reactions, the excess of energy is presumably distributed as vibrational energy in the photoproducts. One of the least understood features of matrix isolation is the detailed nature of photochemical processes therein, including, for example, the cage effect. Some aspects have been discussed elsewhere [25]. The use of photolysis and spectroscopy with plane polarized light has demonstrated that some species can be rotated during the photochemical act. Thus, it seems clear now that all proposed photoproducts **4a**–**e** could be present in the matrix layer studied by Fickert et al. [11,12]. The significant structural differences in the [$FeSiH_2Me$] unit for the mentioned photoproducts should lead to the appearance of new signals in the Raman and IR spectra corresponding to the (FeH) or the (FeC) vibrational modes, or to a shift of (FeSi) and the (SiC) modes. In

this way, one could distinguish between the forms **4a**–**e**. For the compounds **4a**, **4c** and **4e**, the calculations revealed a higher [FeSi] bond order. This leads to a similar shift of the ν(FeSi) mode to higher wavenumbers, as for the iron–carbon single and double bond (Fe–CH_3: 522 cm^{-1}; Fe=CH_2: 624 cm^{-1}) [26]. Table 3 presents the most important theoretically predicted characteristic normal modes of **4a**–**e** and **3a**–**c**, which might help to identify the isolated compound(s) in the matrix experiments performed by Fickert et al. Furthermore, to support this assignment, the calculated IR and, in part, Raman intensities for the different compounds **2a**–**b**, **4a**–**e** and **5** are shown in Table 4. A close examination of the high and low spectral wavenumber region in Table 3 indicates, as expected, different calculated wavenumbers for the before mentioned vibrational modes in **4a**–**e**.

The ν(FeSi) and ν_s(FeCp) modes of **2a**, which have been calculated at 310 and 366 cm^{-1}, were earlier assigned to the strong bands at 318 and 375 cm^{-1}, respectively [11,12]. Whereas these two bands decrease in intensity during the UV irradiation of the sample, a few new bands can be observed in the spectral region between 280–450 and 570–840 cm^{-1}. Consequently the new band at 348 cm^{-1} could be attributed, according to our calculation, to the ν_s(FeCp) mode of **4a** (Calc. 343 cm^{-1}) or to the ν_{as}($CpFeCH_2$) of **4c** (Calc. 346 cm^{-1}). By the comparison of the calculated Raman intensities of these modes, one can observe that a higher signal has been predicted for **4a** than for **2a**, **4b** and **4c**. However, it is also possible that the calculated mode at 314 cm^{-1} for **4b** or 311cm^{-1} for **4c** (see Table 3), which appear in the same region as the ν(FeSi) mode in **2a**, can be overlaped from the mentioned mode

Table 1
Optimized bond lengths (pm) and Angles (°) for compounds **2a**–**5** at BPW91/6-311G* level of theory

	5	**2a**	**2b**	**3a**	**3b**	**3c**	**4a**	**4b**	**4c**	**4d**	**4e**
Distances in pm											
Fe–Is		232.0	–	219.9	231.2	209.7	212.2	230.1	221.6	234.1	211.4
Si–H		150.5	150.4	155.4	152.5	151.6	176.4	149.8	150.3	172.1	151.5
Si–H′		151.0	150.0	150.6	151.1	150.7	151.5	149.4	150.0	149.5	150.9
Si–H″			150.6	–			–			149.4	
Fe–C_1(O_1)	174.0	174.1	174.3	173.9	173.9	173.4	173.4	172.7	173.7	173.8	172.7
C_1–O_1	116.3	116.5	116.2	116.9	116.9	116.8	117.0	116.7	116.9	116.7	116.8
Fe–C_2(O_2)	174.1		174.8	262.2							
C_2–O_2	116.3		116.2	115.0							
Si–C_3		190.5	188.0	188.9	190.3	260.0	188.9	180.7	191.0	181.2	300.6
Fe–H	149.9		–	207.9	302.8	257.2	161.0	148.5	176.1	158.6	
Fe–C_3			207.9	–		210.3		210.9	225.4	209.2	206.8
C_3–H		110.0	110.2	109.8	109.8	110.0	109.7	205.1	116.7		110.0
C_3–H′		110.0	110.2	110.0	110.0	110.0	110.2	109.3	109.6	109.5	109.8
C_3–H″		110.1	–	110.1	110.1	110.1	110.1	109.3	109.6	109.4	110.0
Angles in degree °											
Fe–C_3–Is			117.7			51.7		71.5	63.5	73.3	44.6
Fe–Si–C_3		115.1		129.3	122.2	51.9	130.4	60.3	65.9	58.9	43.4
Si–Fe–C_3						76.5		48.1	50.6	47.9	91.9
Fe–H–Is				72.9	48.2		77.8			90.0	
Fe–H–C_3				–		53.1		67.0	98.6		
C_1–Fe–H	84.8			100.4	113.0	82.7	92.5	82.6	93.9	90.3	
C_1–Fe–Is		85.8		89.2	91.9	92.1	92.5	85.8	89.3	95.9	90.2
C_2–Fe–Is		85.7		109.2							
C_1–Fe–C_3			87.3	–		89.4			95.9	91.6	85.5
Fe–C_1–O_1	178.6	178.6	178.9	175.6	176.7	179.1	178.8		176.8	177.7	179.2
Fe–C_2–O_2	178.3	178.1	177.4	126.8							
C_2–Fe–C_3			91.1								

Table 2
Calculated energy differences in eV and nm between the HOMO and LUMO of the iron complexes

HOMO–LUMO gap	**2a**	**2b**	**3a**	**4a**	**4b**	**4c**	**4d**	**4e**
In eV	3.47	3.18	1.20	2.13	3.47	2.15	2.67	2.10
In nm	357	389	1032	581	357	575	465	591

Table 3
Calculated vibrational wavenumbers (in cm^{-1}) at BPW91/6-311G* for the iron complexes

(2a)	(2b)	(TS3a)	(4a)	(4b)	(4c)	(4d)	(4e)	(5)
2089 [SiH_2]	2154 [SiH_2]	2111 [SiH]	2065 [SiH]	1273 [SiH_2]	2319 [CH_2–H]	2178 [SiH]	2106 [SiH]	
2118 [SiH_2]	2129 [SiH_2]			2143 [SiH_2]		2163 [SiH]	2073 [SiH]	
	2117 [SiH_2]							
		2014 [CO]free		2059 [FeH]	2145 [SiH]			2030 [CO]s
					2120 [SiH]			
2010 [CO]$_s$	2018 [CO]$_s$	1954 [CO]	1960 [CO]	1976 [CO]+[FeH]	1961 [CO]	1974 [CO]	1970 [CO]	1980 [CO]$_{as}$
1970 [CO]$_{as}$	1976 [CO]$_{as}$	1913 [SiH]	1692 [FeH]		1564 [FeH]	1736 [FeH]		1978 [FeH]
1269 [δCH_3]$_s$	1400 [δCH_2]	1272 [δCH_3]$_s$	1264 [δCH_3]$_s$	1397 [δCH_2]$_s$	1363 [δCH_3]$_s$	1403 [δCH_2]$_s$	1231 [δCH_3]$_s$	
1115 [breathing]$_{Cp}$	1117	1111	1111	1116 [breathing]$_{Cp}$	1110	1113 [breathing]$_{Cp}$	1115 [breathing]$_{Cp}$	1114
	[breathing]$_{Cp}$	[breathing]$_{Cp}$	[breathing]$_{Cp}$		[breathing]$_{Cp}$			[breathing]$_{Cp}$
927 [δSiH_2]	931 [δSiH_3]$_{as}$	910	952 [δSiH_2]	930 [δSiH_2]	952 [δSiH_2]	1102 [SiHFe]	978 [δSiH_2]	
		[δSiH]+[ρCH_3]	925[δSiH]			932 [δSiH_2]		
			+[ρCH_3]					
879 [ρCH3]+[ωSiH_2]	926 [δSiH_3]$_{as}$	829 [δSiH_2]	852 [δFeH_{si}]	840	864 [ρCH_3]	885 [ρCH_2]		773 [δCpFeH]
		+[δCH]$_{cp}$		[ρFeH_{CH_3}]+[δCH]$_{cp}$	+[ωSiH_2]	883+[δCH]$_{cp}$ o.o.p.		+[δCH]$_{cp}$
		o.o.p.		o.o.p.				o.o.p.
876 [ρCH3]+[ωSiH_2]	913 [δSiH_3]$_s$	821 [ρCH3]			809 [ρCH_3]	870 [$\omega CH]_{CH_2}$	807 [ρCH_3]	
		+[ωSiH_2]				865 [$\omega CH]_{CH_2}$	803 [ρCH_3]+[δCH]$_{cp}$	
						+[δCH]$_{cp}$ o.o.p.	o.o.p.	
713 [ωSiH_2]+[ωCH_3]	738 [ρCH_2]	702 [$SiCH_3$]	718 [$SiCH_3$]	798 [$SiCH_3$]	659 [SiC]	822 [δCCC]$_{cp}$	770 [ωCH_3]	648 [FeCO]$_s$
663 [$SiCH_3$]+[δFeCO]				765 [δFeH]			623 [FeCO]+[ωSiH_2]	
				659 [ωFeH]+[δFeCO]				
656 [$SiCH_3$]	723 [SiC]	671 [$SiCH_3$]	671 [$SiCH_3$]	616 [ωSiH_2]	626 [ωSiH_2]	797 [$SiCH_2$]	605 [FeCO]+[ωSiH_2]	598 [FeCO]
608 [δFeCO]	649 [$FeCH_2$]	587 [FeCO]	589 [FeCO]	598 [FeCO]+[ωSiH_2]	602 [FeCO]	776 [ωCH_2]	532 [ρSiH_2]+[δFeCO]	554 [δFeCO]
	+[ωSiH_2]				+[ωSiH_2CH_3]			
600 [δFeCO]	645 [δFeCO]	584 [FeCO]	577 [δFeCO]	580 [δFeCO]	594 [δFeCO]	755 [δFeH]	523 [ρSiH_2]+[δFeCO]	531 [δFeCO]
		+[δCC]$_{cp}$						
532 [FeCO]$_s$	597 [δFeCO]	575 [δFeCO]	571 [δFeCO]	574 [δFeCO]+[δCC]$_{cp}$	577 [δFeCO]	672 [ωSiH_2]	495 [$FeCH_3$]	498 [δFeCO]
					+[δCC]$_{cp}$			
515 [FeCO]$_{as}$	522 [FeCO]$_s$	551 [ωSiH_2]		544 [ρSiH_2]	543 [ρSiH_2]	613 [ρSiH_2]+[FeCO]	458 [FeSi]	400 [FeCp]$_{as}$
		+[δCC]$_{cp}$ o.o.p.			536 [τCH_3]			
	516 [FeCO]$_{as}$		521 [ρSiH_2]	485 [τSiH_2]	507 [τSiH_2]	587 [δFeCO]	391 [FeCp]$_{as}$	368 [FeCp]$_{as}$
		416 [FeSi]	434 [FeSi]	444 [$FeSiH_2CH_2$]	435	562 [δFeCO]+[ρSiH_2]	371 [FeCp]$_{as}$	362 [FeCp]$_s$
					[$FeSiH_2CH_3$]			
392 [FeCp]$_{as}$		413 [FeCp]$_{as}$	392 [FeCp]$_{as}$		407 [FeCp]$_{as}$	496 [τSiH_2]+[τCH_2]	338 [FeCp]$_s$	357 [FeCp]$_s$
383 [FeCp]$_{as}$	382 [FeCp]$_{as}$	376 [FeCp]$_{as}$	377 [FeCp]$_{as}$	395 [FeCp]	375 [FeCp]$_{as}$	448 [$FeCH_2$]		
366 [FeCp]$_s$	350 [FeCp]$_s$	323 [FeCpSi]	343 [FeCp]$_s$	375 [FeCp]	346	398 [$FeCpCH_2$]		
					[$FeCH_2Cp$]$_{as}$			
310 [FeSi]	341 [FeCp]$_s$			370 [$FeCpCH_2$]$_s$	311	376 [FeCp]$_s$		
					[$FeCH_2SiH_2$]$_s$			
				314 [$FeCpSiH_2$]$_s$		363 [FeCp]$_{as}$		
						288 [FeSi]		

Table 4
Calculated IR (km mol^{-1}) and Raman ($Å^4$ amu^{-1}) Intensities for the iron complexes at BPW91/6-311G*

	(2a)			(2b)			(TS3a)		(4a)			(4b)			(4c)			(4d)			(4e)			(5)
	IR	R		IR	R		IR		IR	R		IR	R		IR	R		IR	R		IR	R		IR
2118	176.6	158.2	2154	109.4	105.1	2111	135.2	2065	161.3	213.0	2173	114.1	149.4	2319	28.3	41.8	2178	105.9	138.9	2106	164.0	192.3	2030	635.9
2089	136.7	160.2	2129	94.7	99.9	2014	575.6	1960	727.0	28.6	2143	102.9	188.5	2145	147.1	185.3	2163	108.6	224.9	2073	151.1	252.1	1980	773.3
2010	536.0	22.3	2117	190.7	385.0	1954	587.1	1692	151.8	27.4	2059	33.2	74.8	2120	133.9	217.0	1974	708.2	31.6	1970	675.7	36.5	1978	102.1
1970	702.1	43.7	2018	611.6	24.5	1913	14.7	1264	29.6	1.6	1976	657.0	31.9	1961	707.5	32.5	1736	73.4	20.0	1231	20.5	3.4	1114	3.2
1269	19.3	1.4	1976	692.5	46.0	1272	22.4	1111	6.7	51.9	1397	3.9	6.3	1564	43.4	5.3	1403	2.7	6.8	1115	4.3	49.1	773	86.7
1115	2.6	45.6	1400	1.6	9.6	1111	6.1	925	225.7	3.9	1116	3.9	48.7	1363	9.6	5.4	1113	5.4	51.2	978	145.7	8.4	648	37.5
927	94.1	13.0	1117	2.5	44.4	910	111.5	852	4.8	10.8	952	33.4	12.2	1110	7.3	48.7	1102	32.5	10.5	807	2.6	0.9	598	23.8
879	162.5	6.2	931	56.3	27.1	829	64.0	718	113.8	1.4	930	76.4	1.3	952	131.5	10.7	932	114.3	8.8	803	37.9	1.1	554	26.4
876	125.3	4.7	926	27.7	24.4	821	36.8	671	6.8	9.4	840	2.6	26.2	864	104.5	17.1	885	2.7	1.3	623	52.6	3.8	531	0.7
713	59.3	5.7	913	293.7	17.1	702	123.8	589	25.8	6.3	820	32.5	0.6	809	5.9	0.7	883	3.0	1.3	605	55.2	3.5	498	3.0
663	55.5	3.8	738	12.7	2.8	671	7.3	577	17.1	1.8	798	7.8	26.2	659	8.5	16.4	870	12.7	7.1	532	11.6	1.1	400	0.3
656	14.2	12.1	723	8.2	7.0	587	14.5	571	4.6	1.1	765	85.6	3.3	626	60.0	9.1	865	14.4	2.6	523	23.1	2.3	368	2.2
608	28.7	2.9	649	18.7	5.6	575	45.6	521	11.7	6.0	659	103.7	1.0	602	33.4	5.6	822	22.2	1.2	495	1.6	13.5	362	2.3
600	73.8	0.8	645	50.3	2.7	551	80.8	434	0.3	4.9	616	41.2	3.0	594	15.8	2.5	797	10.8	27.5	458	0.3	21.6	357	1.3
532	8.9	9.7	597	42.8	3.0	416	0.9	392	6.2	8.6	598	16.4	8.0	577	18.2	2.6	776	2.1	3.9	391	2.9	11.5		
515	3.9	1.1	522	3.6	7.7	413	30.1	377	4.9	6.5	580	1.7	0.7	543	6.8	4.2	755	2.6	3.9	371	2.3	11.2		
392	4.7	4.9	516	0.5	0.8	376	8.5	343	3.0	28.6	574	18.8	0.1	536	20.3	0.9	672	49.7	9.5	338	1.9	28.1		
383	5.6	4.7	424	1.5	12.4	323	2.7				544	8.7	6.0	507	9.1	7.2	613	45.3	6.9					
366	2.0	11.2	382	2.1	8.9						485	2.9	6.3	435	4.2	1.1	587	49.5	2.2					
310	4.3	19.7	350	0.2	20.2						444	2.8	1.8	407	3.9	7.6	562	7.0	5.6					
			341	3.0	12.7						395	15.4	4.8	375	4.3	7.4	496	7.0	3.6					
											375	8.5	9.7	346	0.7	11.5	448	2.9	2.2					
											370	3.1	13.4	311	2.1	17.7	398	4.6	5.5					
											314	10.3	21.3				376	7.7	7.3					
																	363	6.1	11.2					
																	288	16.6	13.5					

and can not be clearly observed in the Raman spectra, since a similar Raman intensity value has been calculated for these modes (Table 4).

According to our calculations, the strong doublet from 429 and 439 cm^{-1} can be assigned to the ν(FeCp) (Calc. 407 cm^{-1}) and ν(Fe–$\begin{matrix}CH3\\SiH2\end{matrix}$) (Calc. 435 cm^{-1}) modes for **4c** or to the ν(FeCp) (Calc. 392 cm^{-1}) and ν(FeSi) (Calc. 434 cm^{-1}) vibrational modes for **4a**. One may notice that the calculated Raman intensity for the vibrational mode at 392 cm^{-1} in **4a** is much higher than for the corresponding one in **2a**, **4c** and **4b.** Moreover, these experimental results have been supported by the fact that a higher Raman intensity has been calculated, for the theoretical mode at 434 cm^{-1} in **4a** than for the corresponding one in **4b** and **4c** (Table 4).

Using the $\lambda_0 = 514.5$ nm excitation line for photodissociation, these modes and a few new bands in the 500 and 650 cm^{-1} spectral region have been enhanced. This is in good agreement with the orange-red color of the photoproduct, which has been observed in the matrix layer [11,12].

The calculated HOMO–LUMO gaps of the discussed compounds **4a**–**e**, **3a** and **2a**, respectively, are listed in Table 2. The complex **2a** presents an absorption maximum at 363 nm. This band is comparable to the HOMO–LUMO transition of **2a**, which has been calculated at 357 nm (see Table 2). Furthermore, the calculated HOMO–LUMO gaps for the photoproducts **4a** and **4c** are shifted to higher wavelength; this may corresponds to the orange–red colour of the matrix layer and the resonance or preresonance effects observed in the Raman spectrum excited with $\lambda_0 = 514.5$ nm. Surprisingly, the HOMO–LUMO gap of **4b** is much greater than that for **4c** and corresponds to an absorption in the UV spectral region.

A close analysis of the ν(Si–C) wavenumber region could also help to distinguish between the compounds **4a**–**d**. In the Raman spectrum of **2a**, the polarised band at 680 cm^{-1} can be assigned to the ν(Si–C) mode according to the calculated value at 656 cm^{-1}. For the compounds **4b**, **4a**, **3a** and **4c**, these values were determined at 798, 718, 702 and 659 cm^{-1}, respectively.

The assignment of the ν(Si–C) vibrational mode is quite complicated due to the presence of other bands in the same region. However, two new bands of weak intensity could be observed in the Raman spectrum at 702 and 621 cm^{-1} and attributed to this mode. According to the DFT calculations (see Table 3), the new strong bands at 597 and 567 cm^{-1} could be ascribed to the ν(Fe–CO) and δ(FeCO) vibrational modes, respectively.

On the basis of the DFT-calculations the new strong band at 839 cm^{-1} in the Raman spectra of **2a** can be tentatively assigned to the FeH_{Si,CH_3} rocking modes of **4a** (852 cm^{-1}) or **4b** (840 cm^{-1}). One may notice that both have been predicted to show a high Raman band. However, according to the calculated values, this one should be the strongest in the case of **4b** (Table 4).

The detailed analysis of the low-wavenumber region does not offer a determinant factor in distinguishing between the possible isolated photoproduct(s), so that a look on the high wavenumber region, where some changes are also expected, might be decisive.

The Cp ring modes are relatively insensitive to the remaining complex fragment, and, therefore, the Cp ring breathing can be used as internal standard. Indeed, the calculations revealed a deviation of less than 5 cm^{-1} from the experimental value in the title compounds. For the compound **2a**, Fickert et al. [11,12] assigned the week signal at 1249 cm^{-1} (Calc. at 1269 cm^{-1}) to the $\delta(CH_3)$ vibrational mode, as it was expected to occur in the 1200 and 1350 cm^{-1} spectral region. The two new bands, which were not considered by the authors, in fact show up as medium and weak bands at 1302 and at 1341 cm^{-1} [11,12] and seem to play an important role in our characterization. The $\delta_s(CH_3)$ modes for **4a**–**e** were calculated to be at 1264, 1397, 1363, 1403 and 1231 cm^{-1}.

The characteristic SiH_2 modes, as well as the symmetric and antisymmetric CO vibrations in **2a**, which were located at 2090 (br) (Calc. 2118, 2090), 2001 (Calc. 2010) and 1942 cm^{-1} (Calc. 1970), respectively, present a decrease of the intensity during the UV irradiation. The appearance of a new signal at 2136 cm^{-1} in the IR spectrum demonstrates a CO loss, so that the [CpFe(CO)SiH_2Me] equilibrium structures **4a**–**e** were suggested. The broad band at 1942 cm^{-1} splits clearly into two bands after the UV irradiation of **2a**. The new band at 1953 cm^{-1} is increasing, whereas the two ν(CO) bands of **2a** are decreasing. Thus, this band could be assigned to the ν(CO) mode of the photoproducts **4a** and/or **4c**, where both calculated wavenumbers have been found at 1960 cm^{-1}. Furthermore, the new band at 2149 cm^{-1} in the FT–IR spectrum agrees very well with the calculated ν(SiH) modes for **4c** (2145 and 2120 cm^{-1}). The theoretical ν(SiH) mode for **4a**, which has been determined to be 2065 cm^{-1} could not be observed in the reported spectra.

One may notice that the characteristic Fe–H spectral region can certainly help to elucidate the problem in question. According to Tursi and Nixon [27], the medium bands at 1591 and 1600 cm^{-1} observed in the FT–IR spectrum indicate the water's presence in the matrix layer studied by Nagel et al. [10]. But the IR spectrum of **2a** presents two broad bands at 1622 and 1712 cm^{-1} before and after the UV irradiation. The weak band for water, usually expected at around 1630 cm^{-1}, should not be attributed to these strong broad signals. On one hand, during the sample heating in order to bring it in the gas phase, some structural

changes, which could explain these two new signals, can occur. On the other hand, the comparison between those values and the calculated wavenumbers shows a good agreement with the compounds **4a** (1692 cm^{-1}), **4c** (1564 cm^{-1}) and **4d** (1736 cm^{-1}). But one should take into account that the two broad bands could also overlap the ν(FeH), ν(FeHSi) or $\nu(FeHCH_2)$ modes. Thus, the assignment in this region is still under question.

3. Conclusion

The best agreement between the theoretical and experimental data was observed for the ν(CC) modes of the cyclopentadienyl ligand, as well as for the ν(FeSi) and ν(FeCp) low wavenumber vibrational modes. In these cases the discrepancy was only -8 cm^{-1} between experimentally observed and calculated values for **2a**. One may notice that the ν(CO) modes have been also predicted with high accuracy.

The present study has shown that the characteristic vibrational modes of the metal ligand unit for the various photoproducts are significantly different in constitution, but very similar in wavenumbers and in part in intensity. That complicates the differentiation between **4a**, **4b** and **4d** in the experimental results.

Whereas, the new band observed at 839 cm^{-1}, which is attributed to the FeH rocking mode of **4a**, supports the reaction pathway A, the two new bands at 1302 and 1341 cm^{-1} favour the reaction pathway B, whose final product presents a change of the CH_3 unit during the photolysis.

The experimental results seem to support the appearance of compound **4a**, which has been calculated to be the most thermodynamically stable photoproducts. Furthermore, it seems to reveal the presence of compounds **4b**–**c** and/or **4d** too. Indeed, the band which appears at 281 cm^{-1} has not been explained previously [11,12] but with the help of DFT-calculations, it could be tentatively assigned to the ν(FeSi) vibrational mode calculated to be 288 cm^{-1} for **4d**. The calculated Raman intensities of this mode and of the one found at 852 cm^{-1} in **4a** are in the same range, which is in good agreement with the observed experimental result [12]. Moreover, the compound **4d**, for which the theoretical calculations led to the same relative energy as for the isomeric form **4c** (Fig. 1), should be also generated after the photoexcitation of the complex $Cp(CO)_2Fe–CH_2SiH_3$ (2b). Further IR and Raman matrix investigations are recommended for a more certain and correct elucidation of the reaction pathways involved by the irradiation of the title complexes. In this way, matrix investigations of **2b** or of analogous isotopic compounds can prove the presence of **4d** and help to decide if it rearranges to compound(s) **4c** and/or **4a**. To this end, the wavenumbers predicted for the SiD_xCH_x, SiH_xCD_x and SiD_xCD_x ($x = 2$, 3) derivatives complexes have been given as supplementary material together with the HYPERCHEM input files.

4. Computational methods

DFT calculations were performed with the GAUSSIAN 98 series of programs [15]. The 6-311G* [28] basis set has been used for all the atoms with the Becke's 1988 exchange functional [29] in combination with the Perdew–Wang 91 gradient-corrected correlation functional (BPW91) [30]. It has been shown, that new generation of gradient-corrected DFT methods are efficient and accurate methods in studies of transition-metal reactions, especially for treating much larger systems and complexes containing first row transitions metals [31]. The transition states TS were determined with the STQN method (QST2) in GAUSSIAN. The Synchronous Transit-Guided Quasi-Newton (STQN) Method, developed by H. B. Schlegel and coworkers [32], uses a linear synchronous transit or quadratic synchronous transit approach to get closer to the quadratic region around the transition state and then uses a quasi-Newton or eigenvector-following algorithm to complete the optimization. It is well-known that a minimum with all positive eigenvalues in Hessian matrix corresponds to an equilibrium structure, while a saddle point with one negative eigenvalue to a transition-state structure usually connecting two stationary structures. The normal mode corresponding to the imaginary wavenumber of a saddle point must be determined, so that the nature of the TS structure can be analysed. The eigen vectors of the imaginary wavenumber of the TS structure indicate which geometrical parameters are involved in the reaction coordinate (RC). In this respect, the corresponding vibrational mode was animated and studied with the help of the MOLDEN chemical package.

References

[1] W. Malisch, K. Hindahl, H. Käb, J. Reising, W. Adam, F. Prechtl, Chem. Ber. 128 (1995) 963.
[2] (a) D.A. Straus, S.D. Grumbine, T.D. Tilley, J. Am. Chem. Soc. 112 (1990) 7801;
(b) S.D. Grumbine, T.D. Tilley, A.L. Rheingold, J. Am. Chem. Soc. 115 (1993) 358;
(c) S.D. Grumbine, T.D. Tilley, F.P. Arnold, A.L. Rheingold, J. Am. Chem. Soc. 115 (1993) 7884;
(d) S.K. Grumbine, T.D. Tilley, F.P. Arnold, A.L. Rheingold, J. Am. Chem. Soc. 116 (1994) 5495;
(e) S.K. Grumbine, T.D. Tilley, J. Am. Chem. Soc. 116 (1994) 6951;
(f) G.P. Mitchell, T.D. Tilley, J. Am. Chem. Soc. 119 (1997) 11236;

(g) J.D. Feldman, G.P. Mitchell, J.-O. Nolte, T.D. Tilley, J. Am. Chem. Soc. 120 (1998) 11184;
(h) G.P. Mitchell, T.D. Tilley, J. Am. Chem. Soc. 120 (1998) 7635;
(i) G.P. Mitchell, T.D. Tilley, Angew. Chem Int. Ed. 37 (1998) 2524;
(j) S.K. Grumbine, G.P. Mitchell, D.A. Straus, T.D. Tilley, Organometallics 17 (1998) 5607;
(k) J.C. Peters, J.D. Feldman, T.D. Tilley, J. Am. Chem. Soc. 121 (1999) 9871.

[3] (a) M. Denk, R.K. Hayashi, R. West, J. Chem. Soc. Chem. Commun. (1994) 33;
(b) M. Denk, R. West, Pure Appl. Chem. 68 (1996) 785.

[4] B. Gehrhus, P.B. Hitchcock, M.F. Lappert, H. Maciejewski, Organometallics 17 (1998) 5599.

[5] J.M. Dysard, T.D. Tilley, Organometallics 23 (2000) 4726.

[6] B.V. Mork, T.D. Tilley, Abstr. Pap.-Am. Chem. Soc. (2001), 221st INOR-628.

[7] P.W. Wanandi, P.B. Glaser, T.D. Tilley, J. Am. Chem. Soc. 122 (2000) 972.

[8] A. Haynes, M.W. George, M.T. Harward, M. Poliakoff, J.J. Turner, N.M. Boag, M. Green, J. Am. Chem. Soc. 113 (1991) 2011.

[9] K.H. Pannell, T. Kobayashi, F. Cervantes-Lee, Y. Zhang, Organometallics 19 (2000) 351.

[10] V. Nagel, C. Fickert, M. Hofmann, M. Vögler, W. Malisch, W. Kiefer, J. Mol. Struct. 480–481 (1999) 511.

[11] C. Fickert, V. Nagel, W. Kiefer, S. Möller, H. Jehle, W. Malisch, R. Stowasser, G. Bringmann, J. Organomet. Chem. 566 (1998) 225.

[12] C. Fickert, R. Pikl, D. Gernet, S. Möller, W. Malisch, W. Kiefer, Fresenius J. Anal. Chem. 355 (1996) 340.

[13] R.J. Kazlauskas, M.S. Wrighton, Organometallics 1 (1982) 602.

[14] W. Gerhartz, G. Ellerhorst, P. Dahler, P. Eilbracht, Liebigs Ann. Chem. (1980) 1296.

[15] GAUSSIAN 98, Revision A7, M.J. Frisch, G.W. Trucks, H.B. Schlegel, P.M.W. Gill, B.G. Johnson, M.A. Robb, J.R. Cheeseman, T. Keith, G.A. Petersson, J.A. Montgomery, K. Rhaghavachari, M.A. Al-Laham, V.G. Zakrzewski, J.V. Ortiz, J.B. Foresman, J. Ciolowski, B.B. Stefanov, A. Nanayakkara, M. Challacombe, C.Y. Peng, P.Y. Ayala, W. Chen, M.W. Wong, J.L. Andres, E.S. Replogle, R. Gomberts, R.L Martin, D.J. Fox, J.S. Binkley, D.J. Defrees, J. Baker, J.P. Stewart, M. Head-Gordon, C. Gonzalez, J.A. Pople; Gaussian inc., Pittsburg PA, 1998.

[16] Y. Chen, W. Petz, G. Frenking, Organometallics 19 (2000) 2698.

[17] (a) R.S. Simons, C.A. Tessier, Organometallics 15 (1996) 2610;
(b) A.R. Howells, M.C. Milletti, Inorg. Chim. Acta 203 (1993) 43;
(c) D. Braga, F. Grepioni, K. Biradha, G.R. Desiraju, J. Chem. Soc. Dalton Trans. 20 (1996) 3925;
(d) N.J. Fitzpatrick, M.A. McGinn, J. Chem. Soc. Dalton Trans. 8 (1985) 1637;
(e) J.C. Vites, G. Jacobsen, T.K. Dutta, T.P. Fehlner, J. Am. Chem. Soc. 107 (1985) 5563;
(f) B.E. Bursten, R.H. Cayton, Organometallics 5 (1986) 1051.

[18] H.S. Gutowsky, J. Chen, P.J. Hajduk, J.D. Keen, C. Chuang, T. Emilsson, J. Am. Chem. Soc. 113 (1991) 4747.

[19] H.S. Gutowsky, J. Chen, P.J. Hajduk, J.D. Keen, T. Emilsson, J. Am. Chem. Soc. 111 (1989) 1901.

[20] (a) B.K. Campion, R.H. Heyn, T.D. Tilley, J. Am. Chem. Soc. 110 (1988) 7558;
(b) B.K. Campion, R.H. Heyn, T.D. Tilley, A.L. Rheingol, J. Am. Chem. Soc. 115 (1993) 5527.

[21] T.S. Koloski, P.J. Carroll, D.H. Berry, J. Am. Chem. Soc. 112 (1990) 6405.

[22] M.J.S. Dewar, Bull. Soc. Chim. Fr. 18 (1951) C79.

[23] J. Chatt, L.A. Duncanson, J. Chem. Soc. (1953) 2929.

[24] M. Poliakoff, J.J. Turner, J. Chem. Soc. Dalton 1351 (1974) (1973) 2276.

[25] J.K. Burdett, J.J. Turner, in: G.A. Ozin, M. Moskovits (Eds.), Cryogenic Chemistry, Wiley, London, 1976.

[26] S.C. Chang, Z.H. Kafafi, R.H. Hauge, W.E. Billups, J.L. Margrave, J. Am. Chem. Soc. 107 (1985) 1447.

[27] A.J. Tursi, E.R. Nixon, J. Chem. Phys. 52 (1970) 1521.

[28] (a) A.J.H. Wachters, J. Chem. Phys. 52 (1970) 1033;
(b) P.J. Hay, J. Chem. Phys. 66 (1977) 4377;
(c) K. Raghavachari, G.W. Trucks, J. Chem. Phys. 91 (1989) 1062.

[29] A.D. Becke, Phys. Rev. A38 (1988) 3098.

[30] J.P. Perdew, Y. Wang, Phys. Rev. B45 (1992) 13244.

[31] S. Niu, M. Hall, Chem. Rev. 100 (2000) 353.

[32] C. Peng, H.B. Schlegel, Israel J. Chem. 33 (1993) 449.